

## Accepted Manuscript

Title: Simultaneous determination of codeine and its co-formulated drugs acetaminophen and caffeine by utilising cerium oxide nanoparticles modified screen-printed electrode

Authors: Mohamed Khairy, Bahaa G. Mahmouda, Craig E. Banks



PII: S0925-4005(17)32380-8  
DOI: <https://doi.org/10.1016/j.snb.2017.12.054>  
Reference: SNB 23742

To appear in: *Sensors and Actuators B*

Received date: 11-9-2017  
Revised date: 5-12-2017  
Accepted date: 11-12-2017

Please cite this article as: Mohamed Khairy, Bahaa G.Mahmouda, Craig E.Banks, Simultaneous determination of codeine and its co-formulated drugs acetaminophen and caffeine by utilising cerium oxide nanoparticles modified screen-printed electrode, *Sensors and Actuators B: Chemical* <https://doi.org/10.1016/j.snb.2017.12.054>

This is a PDF file of an unedited manuscript that has been accepted for publication. As a service to our customers we are providing this early version of the manuscript. The manuscript will undergo copyediting, typesetting, and review of the resulting proof before it is published in its final form. Please note that during the production process errors may be discovered which could affect the content, and all legal disclaimers that apply to the journal pertain.

**Simultaneous determination of codeine and its co-formulated drugs  
acetaminophen and caffeine by utilising cerium oxide nanoparticles  
modified screen-printed electrode**

Mohamed Khairy,<sup>a\*</sup> Bahaa G. Mahmoud<sup>a</sup> and Craig E. Banks<sup>b</sup>

<sup>a</sup> Chemistry Department, Faculty of Science, Sohag University, 82524.

<sup>b</sup> Faculty of Science and Engineering, Manchester Metropolitan University, Chester Street,  
Manchester M1 5GD, UK.

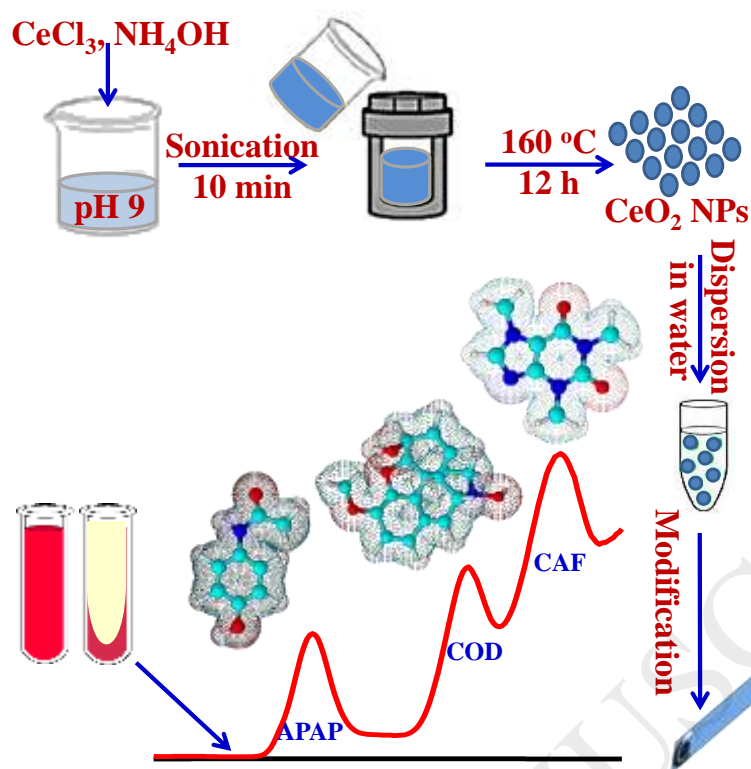
Email: [mohamed.khairy@science.sohag.edu.eg](mailto:mohamed.khairy@science.sohag.edu.eg);

Tel: ++(2)01092099116

**Highlights**

- Simultaneous determination of APAP, COD and CAF on CeO<sub>2</sub>– SPE was explored for the first time.
- CeO<sub>2</sub>-SPE showed high sensitivity, stability and reproducibility compared to unmodified SPE.
- Low detection limits were estimated; 0.051, 0.043 and 2.4 µM for APAP, COD and CAF, respectively.
- CeO<sub>2</sub>-SPE was utilized for simultaneous determinations of APAP, COD and CAF in human fluids.

**Graphical abstract**



Simultaneous determination of acetaminophen, codeine and caffeine drugs using cerium oxide nanoparticles modified screen-printed electrodes (SPEs) is reported for the first time. The CeO<sub>2</sub>-SPEs shows stable, sensitive and reproducible electrochemical non-enzyme sensor without needs any tedious pre-treatment for real samples.

## Abstract

We report a facile and low-cost methodology for simultaneous determination of codeine (COD) and its common co-formulated drugs acetaminophen (APAP) and caffeine (CAF) utilising cerium oxide nanoparticles modified screen-printed electrodes (CeO<sub>2</sub>-SPEs) for the first time. Interestingly, CeO<sub>2</sub>-SPEs offer a promising, sensitive, robust and chemically stable non-enzymatic electrochemical sensor for APAP, COD and CAF determinations without any interference. The electro-analytical sensing of APAP, COD and CAF were explored using CeO<sub>2</sub>-SPEs over a wide concentration range with competitively low detection limits (3S/N) of 0.051, 0.043 and 2.4  $\mu\text{mol L}^{-1}$  respectively. The CeO<sub>2</sub>-SPEs with nanoscale architectures

exhibited practical analytical utilities for accurate simultaneous determination of APAP, COD and CAF in human serum samples with excellent recoveries. The results showed exceptional electrochemical performance of CeO<sub>2</sub>-SPEs in term of simplicity, recyclability, stability and sensing ability that can be effectively reduced processing cost for scalable production and routine analysis.

**Keywords:** Acetaminophen; Codeine; Caffeine; Screen-printed electrode; Cerium oxide nanoparticles; Legal-high drugs.

## 1. Introduction

Disposable graphitic screen-printed electrodes (SPEs) have been extensively used in a plethora of areas, *e.g.* biomedical, pharmaceutical, industrial and environmental field analysis and have been an important field for research and development over recent years [1]. Since they offer a broad palette of electrochemical sensing platforms due to their scales of economy, low cost, easy to use electrodes are realized which are reproducible and can be used as a single-use sensors. Recently, the development of SPEs has become very important particularly for third world countries where the realization of low cost, reliable and portable sensors is imperative for health management and environmental control. However, the selectivity, sensitivity are still the major challenges for electrochemical-based sensor development. Several enzyme-based sensors have been explored. The insufficient stability and reproducibility of enzyme-based sensor has led to establish a variety of artificial enzymes based on nanomaterials that exhibit unexpected enzyme-like activities. Tremendous progress in nano-research has been made by utilizing the unique characteristics of nanoparticles (NPs) [2]. Carbon-based materials; single- and multi-walled carbon nanotube (CNT) and graphene, iron-based nanoparticles;  $\text{Fe}_2\text{O}_3$ ,  $\text{Fe}_3\text{O}_4$ ,  $\text{BiFeO}_3$ ,  $\text{CoFe}_2\text{O}_4$  and  $\text{FeS}$ ,  $\text{NiO}$ ,  $\text{MgO}$ ,  $\text{Co}_3\text{O}_4$ ,  $\text{CdS}$ ,  $\text{TiO}_2$ ,  $\text{BiO}$ , Au NPs, Pt NPs, Ag NPs,  $\text{CuO}$ ,  $\text{ZrO}_2$  and their composites have been explored [3-13]. Although the nanomaterial-based sensors exhibited low cost, easy mass-production, robustness to harsh environments, high stability, long-term storage, tunable activity, size-(shape-, structure-, composition-) dependent properties and large surface area for further modification; low efficiency, specificity and selectivity as well as atomic precise structure and 3D structural information are critically needed [8, 11-13].

Codeine (3-methyl morphine; COD) is an alkaloid belonging to the family of opiates naturally found in the poppy plant [14]. It is a recreational drug has important effects on the central nervous system including analgesic and mood-altering effects. It has long been frequently used as effective opioid analgesic, antitussive, antidiarrheal properties and relieves

severe pain in patients, especially those undergoing surgical procedures [15-16]. COD is a prodrug, itself inactive, but it demethylates to active morphine by the liver enzyme CYP2D6. It absorbs firstly in the gastrointestinal tract then distributes through intravascular spaces to other body tissues with preferential uptake in liver, spleen and kidney. Based on world health organization (WHO) reports, COD is currently the most widely used opiate in the world [17]. COD was found in both single-ingredient and combination preparations commonly with acetaminophen (APAP) and caffeine (CAF).

Acetaminophen (APAP) is one of the most widely common antipyretic and analgesic drugs especially for the patients who are sensitive to acetylsalicylic acid. It is commonly used as a safe and effective painkiller associated with headache, backache, arthritis and postoperative pain due to inhibition of prostaglandin synthesis in the central nervous system [13, 18]. Caffeine (CAF) is an alkaloid belonging to N-methyl derivatives of xanthine that is widely major ingredient of daily beverages and food, such as coffee, tea, Coca-Cola, cola nuts and chocolate. It is used to treat asthma, nasal congestion, and headache or to improve athletic endurance and facilitate weight lost [19]. The combination preparations of APAP, COD and CAF always provide great efficacy for pain relief by about 40% higher than that offered by the same dose of COD alone. These combination drugs can cause depression, sedation and miosis and common symptoms of overdose including nausea, vomiting, skeletal muscle flaccidity, bradycardia, hypotension as well as apnea and death may ensue. Hence, APAP, COD and CAF and their metabolites should be determined in biological fluids for therapy monitoring and screening drug of abuse.

Several analytical methods have been developed for determination of COD and in pharmaceutical dosages and human fluids accurately. High performance liquid chromatography (HPLC) [20, 21], gas chromatography (GC) [22], capillary electrophoresis (CE) [23], flow injection analysis [24], spectrofluorimetry and electrochemical techniques have been reported [25]. Among these analytical techniques, electrochemical method was preferred because it

offers a cost-effective, rapid, and comparatively simple tool for on-site drug determinations. Enzyme-based electrodes have been used for determination of single drug of APAP, COD and CAF drugs; however, multi-fabrication steps, low stability and sensitivity, high cost and narrow concentration range hindered their applicability [26-28]. Thus, design of a sensitive, selective, stable, and reproducible non-enzymatic electrochemical sensor is highly recommended.

In the present manuscript, a simple, sensitive and accurate electroanalytical non-enzyme methodology for the routine simultaneous determination of COD and its common co-formulated drugs APAP and CAF is shown to be possible by utilising cerium oxide ( $\text{CeO}_2$ ) NPs modified SPEs. Towards this goal, a large scale and simple, one-pot hydrothermal synthesis of  $\text{CeO}_2$  NPs has been developed. The  $\text{CeO}_2$ -SPEs exhibit greater electrocatalytic reactivity, higher sensitivity, better stability and reproducibility for simultaneous determination of APAP, COD and CAF molecules over unmodified SPEs. The non-enzyme  $\text{CeO}_2$ -SPEs were successfully employed for ultra-sensitive detection of APAP, COD and CAF concentrations in human fluids.

## 2. Experimental section

### 2.1. Chemicals.

All chemicals were used without any further purification. ( $\text{CeCl}_3$ ; 99.9%) and potassium hexacyanoferrate (II) trihydrate were purchased from Sigma-Aldrich Co. Ltd. Codeine was supplied from Sanofi Aventis Co. Ltd, with purity of 99.17%. Caffeine was obtained from APEX Pharma, Egypt, with purity of 99.17%. Acetaminophen was supplied by Glocal Napi Pharmaceutical Co., Egypt, with purity of 99.31%. All experiments were performed in Britton Robinson (BR) buffer solutions containing 0.05 M of each boric acid, phosphoric acid and acetic acid and 0.1 M sodium hydroxide was added to reach the required pH value. All solutions were prepared by double distilled water ( $> 18 \text{ M}\Omega\cdot\text{cm}$ ).

### 2.2. Synthesis of $\text{CeO}_2$ NPs.

The hydrothermal synthesis of  $\text{CeO}_2$  NPs has been developed using  $\text{CeCl}_3$  and ammonium hydroxide ( $\text{NH}_4\text{OH}$ , 28%) as starting precursors without using any further surfactants. In our synthesis approach, a 1.86 g of  $\text{CeCl}_3$  was dissolved in 50.0 mL deionized water. The transparent solution of  $\text{CeCl}_3$  was introduced into a 100.0 mL Teflon-lined stainless steel autoclave. Then,  $\text{NH}_4\text{OH}$  solution was introduced until a white precipitate was formed. The solution mixture has pH value about 9. The autoclave was sealed and placed in an oven at  $160^\circ\text{C}$  for 12 h for hydrothermal treatment then allowed to cool at room temperature. A white precipitate was formed, collected and rinsed several times with ethanol/water mixture to remove the remaining agents before being dried at  $50^\circ\text{C}$ . Finally, the large yield of  $\text{CeO}_2$  NPs were obtained and stored.

### 2.3. Fabrication of $\text{CeO}_2$ -SPEs.

The screen-printed electrodes, SPEs, were fabricated in-house with appropriate stencil using a DEK 248 screen-printing machine (DEK, Weymouth, U.K.). These electrodes have been used

extensively in previous studies for their fabrication, first, a carbon-graphite ink formulation (product code C2000802P2; Gwent Electronic Materials Ltd., U.K.) was screen-printed onto a polyester (Autostat, 250  $\mu\text{m}$  thickness) flexible film (denoted throughout as standard-SPE); these electrodes have been used extensively in other work [11-13, 29-33]. This layer was cured in a fan oven at 60  $^{\circ}\text{C}$  for 30 min. Next, a silver/silver chloride reference electrode was included by screen-printing Ag/AgCl paste (product code C2040308D2; Gwent Electronic Materials Ltd., U.K.) onto the polyester substrates and a second curing step was undertaken where the electrodes were cured at 60  $^{\circ}\text{C}$  for 30 min. Finally, a dielectric paste (product code D2070423D5; Gwent Electronic Materials Ltd., U.K.) was then printed onto the polyester substrate to cover the connections. After a final curing at 60  $^{\circ}\text{C}$  for 30 min these SPEs are ready to be used. These SPEs have been reported previously and shown to exhibit a heterogeneous electron transfer (HET) rate constant,  $k^{\circ}$ , of ca.  $10^{-3} \text{ cm s}^{-1}$ , as measured using the  $[\text{Ru}(\text{NH}_3)_6]^{3+/2+}$  redox probe.

The  $\text{CeO}_2$  NPs solution was prepared by mixing 80 wt. % of dispersed  $\text{CeO}_2$  NPs and 20 wt. % of graphite in 5.0 mL deionized. The mixture was sonicated for 10 min. 5.0  $\mu\text{L}$  of the mixture was dropped onto the SPEs surface and left it to dry in oven at 50  $^{\circ}\text{C}$  for 30 min.

#### 2.4. Real sample analysis.

Fresh human blood (5.0 mL) was collected from healthy volunteers in the hospital of Sohag University, with the aliquot of the sample collected in a test tube. The collected blood sample was kept at room temperature for 30 min and then centrifuged for 5 min at 3500 rpm. Finally, the supernatant serum sample was collected in a new test tube and stored at 4  $^{\circ}\text{C}$  in a refrigerator when not in use. The APAP, COD and CAF in different concentration levels have been spiked into blood serum sample. Then, the recovery test was carried out by spiking APAP, COD and CAF in serum sample into 20 mL electrochemical cell containing pH 2 B.R buffer and differential pulse voltammetry (DPV) was recorded. A standard addition method was used to determine the APAP, COD and CAF concentrations.

The applicability of CeO<sub>2</sub>-SPEs in selective and sensitive simultaneous determination of COD, APAP, and CAF was investigated. The serum samples were injected with COD, APAP and CAF solutions and then adjusted to pH 2 using small drops of concentration H<sub>2</sub>SO<sub>4</sub>. A 100  $\mu$ L of serum mixture solutions were dropped onto CeO<sub>2</sub>-SPEs surface and DPV signals were recorded. Moreover, the selectivity of CeO<sub>2</sub>-SPEs towards COD, APAP and CAF was tested in presence of various biomolecules such as uric acid, aspirin, glucose, ascorbic acid, dopamine and cysteine in pH 2.

## 2.5 . Characterization of CeO<sub>2</sub> NPs.

The morphology of the CeO<sub>2</sub> sample was investigated using field emission scanning electron microscopy (FE-SEM, JEOL model 6500). The CeO<sub>2</sub> powder was ground and fixed onto a specimen stub using double-sided carbon tape. To obtain high-resolution micrographs, a 10 nm Pt film was coated on the cerium oxide using anion sputtering (Hitachi E-1030) at room temperature. The SEM was operated at 15 KeV to obtain high-resolution SEM images.

Wide-angle powder X-ray diffraction (XRD) was performed by X-ray diffractometer (Model FW 1700 series, Philips, Netherlands) using with monochromatic Cu K $\alpha$  radiation ( $\lambda$  = 1.54 Å), employing a scanning rate of 0.06°/min and 2 $\theta$  ranges from 20° to 80°. The diffraction data were analysed using PDF software Released in 1996.

Thermogravimetric and differential thermal analyses (TG and DTA, respectively) were measured using a simultaneous DTA-TG Apparatus TG-60 (Shimadzu, Japan). A 13 mg of cerium oxide sample was maintained in platinum crucible, heated in nitrogen atmosphere with heating rate of about 5 °C / min.

The Fourier transform infrared (FTIR) spectra of the CeO<sub>2</sub> NPs samples were recorded using Bruker Alpha FTIR instrument in the range 4000 – 400 cm<sup>-1</sup>.

The textural surface properties and pore size distribution was determined by N<sub>2</sub> adsorption / desorption isotherms at 77 K with a BELSORP36 analyzer (JP. BEL Co., Ltd.). The specific surface area ( $S_{\text{BET}}$ ) was calculated using the Brunauer–Emmett–Teller (BET) method with multipoint adsorption data from the linear segment of the N<sub>2</sub> adsorption isotherms. The pore size distribution was determined from the analysis of desorption branch of isotherm using Barrett-Joyner-Halenda (BJH) method.

The voltammetric measurements were carried out using Autolab 302N potentiostat / galvanostat workstation and controlled by NOVA software version 1.11.2 for Windows7.

### 3. Results and discussion

#### 3.1. Features of CeO<sub>2</sub> nanoparticles

Cerium oxide (CeO<sub>2</sub>) is a rare earth element “industrial vitamin” known as ceria and has attracted attention because it has excellent catalytic activities and unique chemical and electronic properties derived from easy conversion of Ce<sup>4+</sup>/Ce<sup>3+</sup> couple. It has ability to store and release oxygen *via* forming and eliminating vacancy defect sites provides an excellent catalyst for many chemical processes [34, 35]. It has been widely used prolifically in many applications such as solid-oxide fuel cells [36], high-temperature oxidation protection materials [37], catalytic materials especially for hydrogen production [38], and removal of CO from the automobile exhaust [39-41], solar cells [42], potential pharmacological agents [43-45] and electrochemical sensors [46]. A simple, one-pot hydrothermal synthesis of CeO<sub>2</sub> NPs has been carried out by adjusting the pH of the CeCl<sub>3</sub> solution by NH<sub>4</sub>OH until a white precipitate was formed without using any structure-directing agent. Figure 1(a, and b) shows typical SEM images of CeO<sub>2</sub> sample synthesized by the facile hydrothermal synthesis described in the experimental section. The SEM images exhibited nano-sized CeO<sub>2</sub> particles with sphere-like morphology with an average diameter of 40 nm. The crystal structure of CeO<sub>2</sub> powder was characterized using XRD and is shown in Figure 1(c). Well-resolved and distinct diffraction peaks have been indexed with corresponding (hkl) values using JCPDS data file (04-0593) indicating single nano-crystalline structure of CeO<sub>2</sub>. These diffraction peaks coincided with the face-centered cubic (*Fm3m*) symmetry. Interestingly, our protocol provides facile methodology and template-free to synthesize highly crystalline CeO<sub>2</sub> NPs. The thermal decomposition of as-synthesised CeO<sub>2</sub> NPs was studied using thermogravimetry-differential thermal analysis (TG-DTA) techniques. The TGA profile (Figure 1d) revealed formation of CeO<sub>2</sub> NPs upon hydrothermal treatment and no thermal treatment was required. The TGA of CeO<sub>2</sub> nanoparticle displays a weight loss about 1.126 % below 150 °C, indicating elimination of the physically absorbed water. The loss of weight about 1.982 % in the temperature range of 150 – 400 °C

mainly attributed to crystallization water. The slightly decreased in TGA curve was accompanied by an exothermic peak in the corresponding DTA curve at 240 °C, indicates the presence of trace amount of  $\text{Ce}(\text{OH})_4$  or associated water after hydrothermal treatment.

**Figure 1**

To determine the surface functional groups of  $\text{CeO}_2$  NPs, FTIR spectra was performed and shown in Figure 2a. The  $\text{CeO}_2$  NPs show absorption bands around 450 to 700  $\text{cm}^{-1}$ , corresponding to Ce-O stretching vibration which confirm the formation of  $\text{CeO}_2$  NPs. Whereas the band at 3410 and 1620  $\text{cm}^{-1}$  are assigned to the stretching and bending mode of the hydroxyl group, indicates of the presence of residual water and hydroxyl groups in  $\text{CeO}_2$  NP; which is agree with TGA analysis (Figure 1d). The absorption bands at 1437  $\text{cm}^{-1}$  is might attributed to deformation mode of ammonium ions. The peak at 1045  $\text{cm}^{-1}$  can be assigned Ce-O-C stretching vibration which evidently proves presence of carbon on the  $\text{CeO}_2$  nanoparticles because the hydrothermal synthesis was not carried out in a free  $\text{CO}_2$  atmosphere [47]. The specific surface area and porosity of the  $\text{CeO}_2$  NPs were investigated by using  $\text{N}_2$  adsorption/desorption isotherms. Figure 2 shows the  $\text{N}_2$  adsorption/desorption isotherms and the corresponding Barrett-Joyner-Halenda (BJH) pore-size distribution. The as-synthesized  $\text{CeO}_2$  sample exhibits a BET specific surface area of 40.2  $\text{m}^2\text{g}^{-1}$  and a total pore volume of 0.286  $\text{cm}^3\text{g}^{-1}$  with relatively broad pore size distribution in range of 61 - 86 nm, calculated from the desorption branch. The porous network texture of  $\text{CeO}_2$  NPs is very important for designing an electrochemical non-enzymatic sensor because it provides an enhanced surface area over that of a bare SPE with changes in mass transport characteristics which results in sensitivity enhancements [11, 13].

**Figure 2**

### 3.2. Electrochemical characterization of $\text{CeO}_2$ NPs.

The electrocatalytic performance of CeO<sub>2</sub> modified screen-printed electrode (CeO<sub>2</sub>-SPE) was explored by using cyclic voltammetry (CV) and electrochemical impedance spectroscopy. Figure 3 (a, and b) shows cyclic voltammetric curves and Nyquist plots of CeO<sub>2</sub>-SPE and unmodified/bare SPE in a redox couple of 0.5 mM K<sub>4</sub>[Fe(CN)<sub>6</sub>]/ K<sub>3</sub>[Fe(CN)<sub>6</sub>] and 0.1 M KCl as supporting electrolyte. From analysis of the CV curves, the peak potential shifts  $\approx$  50 mV to less positive potentials. The peak separations are about 0.264 V and 0.314 V for CeO<sub>2</sub>-SPE and unmodified SPE at scan rate of 0.05 V/s, respectively. Moreover, the peak current was significantly improved. The effect of CeO<sub>2</sub> nanoparticles upon the SPE's heterogeneous electron transfer process can be explored by employing Nicholson's method. It is widely used to estimate the heterogeneous rate constant ( $k^\circ$ ) for quasi-reversible electrochemical reactions *via* the following equation [48]:

$$\Psi = k^\circ \{\pi D n \nu F / RT\}^{-1/2}$$

where  $\Psi$  is a kinetic parameter,  $D$  is the diffusion coefficient for [Fe(CN)<sub>6</sub>]<sup>3-/4-</sup> ( $7.60 \times 10^{-6}$  cm<sup>2</sup> s<sup>-1</sup>),  $n$  is the number of electrons transferred in the reaction,  $\nu$  is the scan rate,  $F$  is the faraday constant,  $R$  is the gas constant, and  $T$  is the Temperature (Kelvin).  $\Psi$  is deduced from  $\Delta E_P$  (the *peak-to-peak* separation) for a one electron process at a set temperature (298 K). For practical usage, the function of  $\Psi(\Delta E_P)$  could fits Nicholson's data as given by:  $\Psi = (-0.6288 + 0.0021X)/(1 - 0.017X)$ , where  $X = \Delta E_P$  is used to determine  $\Psi$  as a function of experimentally obtained  $\Delta E_P$  values at various voltammetric scan rates. It is therefore possible to produce a graph, whereby  $\Psi$  is plotted against  $[\pi D n \nu F / RT]^{-1/2}$ , and the standard heterogeneous rate constant ( $k^\circ$ ) can be determined *via* the gradient. In cases where the  $\Delta E_P$  exceeds a value of 212 mV, the following equation should be considered:

$$\text{where } \alpha \text{ is } k^\circ = [2.18(\alpha D n \nu F / RT)^{1/2}] \text{Exp}[-(\frac{\alpha^2 n F}{RT})x \Delta E_p] \text{ assumed to be 0.5.}$$

The heterogeneous charge transfer rate constants were estimated to be  $1.80 \times 10^{-4}$  and  $3.20 \times 10^{-4}$  cm. s<sup>-1</sup> for SPE and CeO<sub>2</sub>-SPE, respectively. These results demonstrate the electrocatalytic efficiency of CeO<sub>2</sub> nanoparticles that facilitate the charge transfer rate of

the graphite screen-printed electrode in order of 2 times. To measure the electrochemically active surface area of the unmodified SPE and CeO<sub>2</sub>-SPE, the chronoamperogram of 1.0 mM [Fe(CN)<sub>6</sub>]<sup>3-/4-</sup> as a redox probe in 0.1 M KCl was recorded. The diffusion current is described by Cottrell equation [49];

$$I_d(t) = \frac{nFAD^{1/2}C_o^*}{\pi^{1/2}t^{1/2}}$$

where  $n$  is the number of electrons transferred in the reaction,  $F$  is the Faraday constant,  $A$  is the electrochemical active area,  $D$  is the diffusion coefficient and  $C$  is the bulk concentration. Under diffusion control, a plot of  $I$  vs.  $t^{-1/2}$  will be linear and the surface areas was calculated to be  $5.12 \times 10^{-2}$  and  $6.73 \times 10^{-2}$  cm<sup>2</sup> for unmodified SPE and CeO<sub>2</sub>-SPE, respectively.

The EIS an efficient method was used to study the interface properties of the modified electrodes. Figure 3b shows Nyquist plots of CeO<sub>2</sub>-SPE and unmodified in [Fe(CN)<sub>6</sub>]<sup>3-/4-</sup> / 0.1 M KCl system; the applied DC-voltage is about 0.3 V (vs. Ag/AgCl), the excitation AC voltage applied to the electrochemical cell was 5 mV (*peak-to-peak*), and the frequency range was from 100 kHz to 0.1 Hz. The impedance plot consists of a semicircular part related to direct electron transfer process of the SPEs and [Fe(CN)<sub>6</sub>]<sup>3-/4-</sup> and a linear part with angle 45 °C related to diffusion control of [Fe(CN)<sub>6</sub>]<sup>3-/4-</sup> species at lower frequencies. Based on the charge transfer kinetics of [Fe(CN)<sub>6</sub>]<sup>3-/4-</sup> redox probe, the faradic impedance of unmodified and CeO<sub>2</sub>-SPE can be described by the Randles's equivalent circuit. The Randles's equivalent circuit usually contains solution resistance (R1), constant phase element (CPE1) was modeled as a non-ideal capacitor, Warburg impedance (W1), and charge transfer resistance (R2) (inset Figure 3b). As shown in Table 1, the solution resistance was slightly increased in the presence of the CeO<sub>2</sub> layers, which indicates a good electron conductor covers the SPEs surface [50]. This also confirmed by the numerical values of charge transfer resistance, that decreases by half of its original value of unmodified SPEs. This result is very consistent with CV data for

heterogeneous charge transfer rate values. Consequently, the Warburg impedance value of CeO<sub>2</sub>-SPE was decreased and capacitance was slightly increased. This result indicates an effective charge transfer at SPE surface via CeO<sub>2</sub> NPs-mediated charge transfer mechanism.

**Figure 3**

### 3.3. Electrochemical behaviours of APAP, COD and CAF on CeO<sub>2</sub>-SPE.

The electrochemical behaviour of APAP, COD and CAF were investigated on unmodified SPE and CeO<sub>2</sub>-SPE using CV and differential pulse voltammetry (DPV). For example, differential pulse voltammograms of 50  $\mu\text{mol L}^{-1}$  COD on different metal oxide NPs modified SPEs were shown in Figure S1A. Among the metal oxide nanoparticles used [51], CeO<sub>2</sub> NPs modified SPE shows an interesting electrochemical response for COD in pH 2.0 (Figure S2). COD is weak base; its pK<sub>a</sub> value is about 7.9, above this value the COD was existed in deprotonated form which exhibits a net negative charge. Therefore, the protonated form of COD is important and desirable for oxidation on CeO<sub>2</sub>-SPE. Next, chronoamperometric measurements of COD at CeO<sub>2</sub>-SPE were carried out by employing single step potential of 1.14 V vs. Ag/AgCl for different concentrations of COD in B.R. buffer solution of pH 2.0. At the mass transport limiting conditions, the current is proportional to  $t^{-1/2}$  and fitted Cottrell equation [49]. From the slop values, the average value of diffusion coefficient D was calculated to be  $4.93 \times 10^{-5} \text{ cm}^2/\text{s}$ . The chronoamperometric method and Galus equation can be used also for determination of the catalytic rate constant,  $k_{cat}$  [52].

$$\frac{I_{cat}}{I_d} = \gamma^{1/2} [\pi^{1/2} \text{erf}(\gamma^{1/2}) + \frac{\exp(-\gamma)}{\gamma^{1/2}}] = \gamma^{1/2} \pi^{1/2} = \pi^{1/2} (kCt)^{1/2}$$

where  $I_{cat}$  is the catalytic current of CeO<sub>2</sub> NPs in presence of COD and  $I_d$  is limited current in absence of COD,  $\gamma$  is the argument of the error function, if  $\gamma > 2$ ; the  $\text{erf}(\gamma^{1/2})=1$ , C is the bulk concentration of COD and t is the time elapsed. The catalytic rate constant was calculated to be  $1.66 \times 10^5 \text{ L mol}^{-1} \text{ s}^{-1}$  from the slops of the linear plot of  $I_{cat}/I_d$  vs.  $t^{1/2}$ .

The cyclic voltammetric curves for 100  $\mu\text{mol L}^{-1}$  APAP, 100  $\mu\text{mol L}^{-1}$  COD and 100  $\mu\text{mol L}^{-1}$  in B. R. buffer solution (pH 2.0) on unmodified SPE and  $\text{CeO}_2$ -SPE (Figure S1B). A three distinctive voltammetric oxidation peaks were depicted in both unmodified SPE and  $\text{CeO}_2$ -SPE. The peak potentials of APAP, COD and CAF on unmodified SPEs were 0.64 V, 1.22 V and 1.48 V respectively; while, the peak potentials of APAP, COD and CAF on  $\text{CeO}_2$ -SPE were 0.6 V, 1.14 V and 1.42 V (vs. Ag/AgCl), respectively. A significant negative potential shift for APAP, COD and CAF with improved in oxidation peak currents were observed for  $\text{CeO}_2$ -SPE. This result indicates that  $\text{CeO}_2$  NP is a good electro-catalyst as well as could be used for simultaneous determination of APAP, COD and CAF molecules.

Next, we turned to study the effect of scan rate upon the electrochemical oxidation behaviours of APAP, COD and CAF in B.R. buffer pH 2.0. Figure 4 shows the cyclic voltammetric curves of 100  $\mu\text{mol L}^{-1}$  APAP, 200  $\mu\text{mol L}^{-1}$  COD and 200  $\mu\text{mol L}^{-1}$  in pH 2.0 in various scan rate in the range of 0.01 – 0.5  $\text{Vs}^{-1}$ . No reduction peaks have been observed in the cyclic voltammograms of COD and CAF. However, the intensity of APAP reduction peak becomes significant at higher scan rates. Meanwhile, there was a positive shift of peak potentials with the increase of scan rate. The analysis of peak height against the square-root of scan rate was found to be linear indicating a diffusional controlled processes (For APAP;  $I_{\text{pa}}/\mu\text{A} = 0.188 v^{1/2} + 0.154 \mu\text{A}$ ,  $R^2 = 0.983$ , For COD;  $I_{\text{pa}}/\mu\text{A} = 0.16 v^{1/2} + 0.61 \mu\text{A}$ ,  $R^2 = 0.98$ , For CAF;  $I_{\text{pa}}/\mu\text{A} = 0.193 v^{1/2} + 0.346 \mu\text{A}$ ,  $R^2 = 0.99$ ). The variations of the oxidation peak heights of APAP, COD and CAF with different scan rates were not linear. Moreover, the linear relationship of  $\log(I_{\text{pa}})$  and  $\log v$  can be expressed as following; For APAP;  $\log I_{\text{pa}} = 0.42 \log v - 0.52$ , For COD;  $\log I_{\text{pa}} = 0.36 \log v - 0.36$ , For CAF;  $\log I_{\text{pa}} = 0.42 \log v - 0.49$ . The slope values which corresponding to heterogeneous charge transfer coefficient ( $\alpha$ ) are very close to the theoretical value of 0.5, which clearly indicates that the electrochemical response is controlled by diffusional mass transfer processes (Figure S3). This result indicated that, no significant adsorption of APAP, COD and CAF molecules at  $\text{CeO}_2$ -SPE which reveal long-term stability and signal reproducibility even after several voltammetric cycles. This behaviour

is rarely observed as electrochemical processes are surface controlled [48-50, 53- 65]. The number of electrons transferred in the electro-oxidation processes of APAP, COD and CAF can be estimated by applying the following equation:  $E_p - E_{p/2} = 47.7 \text{ mV}/\alpha n$ . The values of  $E_p - E_{p/2}$  is about 0.051, 0.07 and 0.05 V for APAP, COD and CAF, respectively, the number of electrons transferred ( $n$ ) was estimated to be equals to 2 for APAP, COD and CAF drugs. Further, the current functions ( $I_{pa}C/v^{1/2}$ ) of APAP, COD and CAF were exponentially decay with increasing scan rates, indicating that the  $E_rC_{irr}$ -mechanism is dominated the electro-oxidation of APAP, COD and CAF molecules.

Since the selection of pH is very important in electroanalysis, the effect of solution pHs upon the electrochemical signals of APAP, COD and CAF. Figure S4 shows differential pulse voltammetric responses of  $50 \mu\text{mol L}^{-1}$  APAP and  $50 \mu\text{mol L}^{-1}$  COD and  $50 \mu\text{mol L}^{-1}$  on CeO<sub>2</sub>-SPE in B. R. buffer of different pHs. With increasing the pH values, the oxidation potentials of APAP, COD and CAF are shifted to less positive values, the peak current of APAP is decreased, the peak of COD split into two consecutive waves and CAF is difficult to detect. This result indicates that, the B.R. buffer pH 2.0 is the optimum medium for simultaneous determination of APAP, COD and CAF. The slope of linear relationship between  $E_p$  and pH was found to be 45 mV/pH, 54 mV/pH and 51 mV/pH for APAP, COD and CAF, respectively. These values are very close to Nernstian slope (59 mV/pH at 298 K) for a process that involves the transfer an equal number of protons and electrons in the electrochemical mechanism. From the above results the electro-oxidation mechanisms of APAP [13, 48], CAF [49] and COD [50] molecules can be described as follows (Scheme 1).

#### Scheme 1

#### Figure 4

### 3.4. Electrochemical determination of APAP, COD and CAF.

Differential pulse voltammetry (DPV) technique was employed to obtain the linear ranges and detection limits for the APAP, COD and CAF drugs. Several DPV parameters including deposition time, equilibrium time, modulation time and amplitude were investigated to find out optimum parameters for simultaneous determination of APAP, COD and CAF on CeO<sub>2</sub>-SPE. Figure S5 shows the differential pulse voltammograms of 50  $\mu\text{mol L}^{-1}$  APAP and 50  $\mu\text{mol L}^{-1}$  COD and 50  $\mu\text{mol L}^{-1}$  onto CeO<sub>2</sub>-SPE. The DPV experiments were recorded using the following parameters; step potential 0.01 V, modulation potential 0.025 V, modulation time 0.05s, interval time 0.2 s, scan rate 50 mVs<sup>-1</sup>, deposition time 20 s and equilibrium time 20 s. Figure 5 displays the DPV responses of the electrochemical oxidation of APAP, COD and CAF on CeO<sub>2</sub>-SPE in B.R. buffer pH 2.0 under the optimized working conditions. The peak height was increased with continuous additions of APAP, COD and CAF solutions. For APAP, two linear relationships were established (as shown in Figure 5B) in the range of 0.09 to 7.0  $\mu\text{mol L}^{-1}$  and 16.4 to 1160  $\mu\text{mol L}^{-1}$  as  $I_p (\mu\text{A}) = 0.446 C_{\text{APAP}} + 0.164 \mu\text{A}$  ( $R^2 = 0.99$ ) and  $I_p (\mu\text{A}) = 0.006 C_{\text{APAP}} + 3.03 \mu\text{A}$  ( $R^2 = 0.98$ ), respectively. Two linear segments of COD were also presented (as shown in Figure 5D) in the range of 0.09 to 50  $\mu\text{mol L}^{-1}$  and 120 to 500  $\mu\text{mol L}^{-1}$  as  $I_p (\mu\text{A}) = 0.04 C_{\text{COD}} + 0.014 \mu\text{A}$  ( $R^2 = 0.99$ ) and  $I_p (\mu\text{A}) = 0.006 C_{\text{COD}} + 1.8 \mu\text{A}$  ( $R^2 = 0.97$ ), respectively. Also two linear range of CAF concentrations were obtained as shown in Figure 5F in the range of 5 to 286  $\mu\text{mol L}^{-1}$  and 387 to 916  $\mu\text{mol L}^{-1}$  as  $I_p (\mu\text{A}) = 0.0108 C_{\text{CAF}} + 0.122 \mu\text{A}$  ( $R^2 = 0.99$ ) and  $I_p (\mu\text{A}) = 0.0046 C_{\text{CAF}} + 2.05 \mu\text{A}$  ( $R^2 = 0.98$ ), respectively. Based on the first linear fitting equations of APAP, COD and CAF, the limits of detection were calculated to be  $51 \times 10^{-9}$  M,  $43 \times 10^{-9}$  M and  $2.4 \times 10^{-6}$  mol L<sup>-1</sup>, respectively. The superior performance of the CeO<sub>2</sub>-SPE suggests a promising platform for simultaneous electrochemical determination of APAP, COD and CAF recreational drugs.

**Figure 5**

As mentioned previously, simultaneous determination of APAP, COD and CAF were studied in different pH values (Figure S4), and B.R. buffer pH 2.0 was selected as optimum

conditions. DPV for successive additions of APAP in presence of 50  $\mu\text{mol L}^{-1}$  COD and 50  $\mu\text{mol L}^{-1}$  CAF revealed that three separate and distinct peaks of APAP, COD and CAF were observed (Figure 6A). Interestingly, there is no any significant change in the voltammetric response of COD and CAF with consequence additions of APAP. The calibration curve of APAP was shown in Figure 6B with two linear relationship from 0.09 to 100.0  $\mu\text{mol L}^{-1}$  with a linear equation;  $I_p (\mu\text{A}) = 0.052 C_{\text{APAP}} + 0.405 \mu\text{A}$  ( $R^2 = 0.99$ ) and linear range from 150.0 to 570.0  $\mu\text{mol L}^{-1}$  with a linear equation;  $I_p (\mu\text{A}) = 0.01 C_{\text{APAP}} + 5.5 \mu\text{A}$  ( $R^2 = 0.97$ ). The DPV for successive additions of COD in presence of 50  $\mu\text{mol L}^{-1}$  APAP and 50  $\mu\text{mol L}^{-1}$  CAF was shown in Figure 6C. No significant change in the current responses of APAP and COD. A calibration curve for additions of COD was presented in Figure 6D with two linear relationships from 0.09 to 20  $\mu\text{mol L}^{-1}$  with a linear equation;  $I_p (\mu\text{A}) = 0.09 C_{\text{COD}} + 0.41 \mu\text{A}$  ( $R^2 = 0.993$ ) and from 50 to 1229  $\mu\text{mol L}^{-1}$  with a linear equation;  $I_p (\mu\text{A}) = 0.005 C_{\text{COD}} + 2.29 \mu\text{A}$  ( $R^2 = 0.984$ ). Also, Figure 6E shows successive additions of CAF in presence of 50  $\mu\text{mol L}^{-1}$  APAP and 50  $\mu\text{mol L}^{-1}$  COD drugs. No significant changes for APAP and COD current responses. Two linear calibration curves for addition of CAF were presented in Figure 6F as following; from 5 to 476  $\mu\text{mol L}^{-1}$  with a linear equation;  $I_p (\mu\text{A}) = 0.01 C_{\text{CAF}} + 0.588 \mu\text{A}$  ( $R^2 = 0.988$ ) and from 568 to 1234  $\mu\text{mol L}^{-1}$  with a linear equation;  $I_p (\mu\text{A}) = 0.0033 C_{\text{CAF}} + 3.93 \mu\text{A}$  ( $R^2 = 0.997$ ). These results synergistically proved the feasibility of  $\text{CeO}_2$  - SPEs for simultaneous determination and distinguished electrochemical sensing performance for APAP, COD and CAF recreational drugs (Table 2 and Figure S9). While the  $\text{CeO}_2$ -SPE offers many advantages over previous literatures [48-60] such as simple fabrication process, large-scale production, low cost, no need any pre-treatment and can be used in wide concentration ranges of APAP, COD and CAF with high stability, sensitivity and reproducibility for on-site field analysis.

**Figure 6**

**Table 2**

### 3.5. Costless, stable and reproducible CeO<sub>2</sub>-SPE sensor for simultaneous determination APAP, COD and CAF drugs.

Screen-printed electrodes (SPEs) are widely used in various biomedical and environmental analyses because they provide a low cost, single-shot disposable yet highly reproducible and reliable platform for electrochemical sensing of various analyte. The reproducibility of CeO<sub>2</sub>-SPE was investigated by using the same electrode for 5 repetitive measurements of 50  $\mu\text{mol L}^{-1}$  APAP, 50  $\mu\text{mol L}^{-1}$  COD and 50  $\mu\text{mol L}^{-1}$  CAF in pH 2.0. The relative standard deviation was calculated to be 1.28 %, 1.41 % and 1.52 % for APAP, COD and CAF respectively. Furthermore, CeO<sub>2</sub> - SPE shows not only reproducible signal on the same electrode but also with separately employed electrodes. Three electrodes were examined in presence of 50  $\mu\text{mol L}^{-1}$  APAP, 50  $\mu\text{mol L}^{-1}$  COD and 50  $\mu\text{mol L}^{-1}$  CAF under the same conditions. The relative standard deviation was calculated to be 2.28 %, 1.36 % and 3.6 % for APAP, COD and CAF drugs, respectively. After one month of storage, the CeO<sub>2</sub>-SPE was also examined in presence of 50  $\mu\text{mol L}^{-1}$  APAP, 50  $\mu\text{mol L}^{-1}$  COD and 50  $\mu\text{mol L}^{-1}$  CAF in B.R. buffer pH 2.0. CeO<sub>2</sub>-SPE showed high stability of the differential pulse voltammetric waves over one month of storage with relative standard deviation less than 2.34 %.

### 3.6. Analysis of real samples and interferences.

To verify the applicability of CeO<sub>2</sub>-SPE sensor, the voltammetric recovery experiment of APAP, COD and CAF in human serums were performed as in experimental section 2.4. Before DPV determination, the APAP, COD and CAF were spiked into human serum samples and left them for 30 min in fridge at 4 °C. Then, these spiked samples were added to 20 mL electrochemical cell containing B. R. buffer pH 2.0. The concentrations of APAP, COD and CAF were determined by standard addition method. The results are summarized and listed in Table 3. Satisfactory recovery experiment for human serum samples demonstrated that the CeO<sub>2</sub>-SPE held great promise for reliable and sensitive simultaneous determination of APAP, COD and CAF in the clinical analysis.

**Table 3**

Various electroactive species that potentially interfere with the determination of APAP, COD and CAF were investigated under optimum conditions of B.R. buffer pH 2.0 on CeO<sub>2</sub>-SPE. Figure S6 shows consecutive additions of 50  $\mu\text{mol L}^{-1}$  APAP, 50  $\mu\text{mol L}^{-1}$  COD, 75  $\mu\text{mol L}^{-1}$  CAF, 500  $\mu\text{mol L}^{-1}$  glucose, 500  $\mu\text{mol L}^{-1}$  ascorbic, 200  $\mu\text{mol L}^{-1}$  uric acid, 50  $\mu\text{mol L}^{-1}$  aspirin on only one electrode of CeO<sub>2</sub>-SPE in the B.R. buffer pH 2.0. It is worthy noted that, the presence of higher concentrations of glucose, ascorbic, uric acid and aspirin molecules does not interfere with APAP, COD and CAF. The tolerance limit was calculated to be less than  $\pm 4\%$ . Interestingly, the CeO<sub>2</sub>-SPE showed high specificity, stability and sensitivity for determination of APAP, COD and CAF even in presence of interferences. Further, CeO<sub>2</sub> NPs has been used previously for oxidation of dopamine and cysteine [34,35]. Figure S7 showed simultaneous additions of 50  $\mu\text{mol L}^{-1}$  APAP, 50  $\mu\text{mol L}^{-1}$  COD, 50  $\mu\text{mol L}^{-1}$  CAF, 100  $\mu\text{mol L}^{-1}$  Dopamine and 100  $\mu\text{mol L}^{-1}$  Cysteine. Dopamine does not effect on the peak height of APAP, COD and CAF and also can be determine simultaneously in presence of these drugs. Cysteine interferes slightly with CAF in presence of CeO<sub>2</sub> NPs on SPE. Consecutive additions of morphine (MOR) drug in B.R. buffer pH 2.0 in presence of 50  $\mu\text{mol L}^{-1}$  APAP, 50  $\mu\text{mol L}^{-1}$  COD, 50  $\mu\text{mol L}^{-1}$  CAF was shown in Figure S8. Interestingly, CeO<sub>2</sub>-SPE showed high sensitivity and selectively determination of APAP, COD and CAF in presence of MOR, dopamine and cysteine molecules compared to unmodified SPEs.

**Figure 7**

In order to test the applicability of CeO<sub>2</sub>-SPE in measurements of APAP, COD, and CAF in human fluids, the APAP, COD and CAF with different concentration were injected to serum samples. The samples were adjusted by little drops of H<sub>2</sub>SO<sub>4</sub> to reach pH 2. A 100  $\mu\text{L}$  of serum containing drugs were dropped onto CeO<sub>2</sub>-SPE surface. Hence, three-electrode configuration cell of the screen printed electrode was used; CeO<sub>2</sub> modified carbon is working electrode, Ag/AgCl as pseudo-reference electrode and carbon as counter electrode. DPV current signals

were recorded as shown in Figure 7. Therefore, a simple, cheap, reliable and sensitive electrochemical sensor based on CeO<sub>2</sub> NPs shows merits over prior art, which is applicable for simultaneous sensing of APAP, COD and CAF in presence of interferences in biological applications.

## Conclusions

A simple and one –pot hydrothermal synthesis of CeO<sub>2</sub> NPs has been developed and used for simultaneous determination of APAP, COD and CAF for the first time as a non-enzymatic sensor. The CeO<sub>2</sub> NPs are simply casted onto SPEs mutually facilitate the electron transfer and mass transport as well as electrocatalytic activity. The CeO<sub>2</sub> NPs remarkably decreased overvoltage and improved electrochemical response of APAP, COD and CAF in term of specificity, sensitivity and selectivity. Furthermore, the CeO<sub>2</sub>–SPE was applied for the determination of APAP, COD and CAF in human serum directly without any treatment or even filtration with satisfying results, indicating that CeO<sub>2</sub>-SPE can be a promising electrode material for on-site determination of APAP, COD and CAF recreational drugs.

## ACKNOWLEDGEMENTS:

The authors acknowledge funding from a British Council Institutional Link grant and Science and Technology Development Fund in Egypt (STDF) (No. 172726574, Project ID 18435) for the support of this research.

## References

1. D.A. C. Brownson, D. K. Kampouris and C. E. Banks, *Chem. Soc. Rev.*, 41 (2012) 6944-6976
2. H. Wei and E. Wang, *Chem. Soc. Rev.*, 42 (2013) 6060-6090.
3. A. Chen and S. Chatterjee, *Chem. Soc. Rev.*, 42 (2013) 5425.
4. M. Khairy, A. A. Khorshed, F. A. Rashwan, G. A. Salah, C. E. Banks, *Sens. Actuators, B*, 252 (2017) 1045-1054.
5. Y. Wang, L. Wang, H. Chen, X. Hu, and S. Ma, *ACS Appl. Mater. Interfaces*, 8 (2016) 18173–18181.
6. G. Liu and Y. Lin, *Anal. Chem.*, 77 (2005) 5894–5901.
7. L. Hu, C-Chun. Fong, X. Zhang, L. L. Chan, P. K. S. Lam, P. K. Chu, K-Yin. Wong, and M. Yang, *Environ. Sci. Technol.*, 50 (2016) 4430–4438.
8. M. Khairy, S. A. El-Safty, *Sens. Actuators, B*, 193 (2014) 644–652.
9. J. A. Hansen, V.V. Sumbayev and K.V. Gothelf, *Nano Lett.*, 7 (2007) 2831–2834.
10. P. K. Kannan, D. J. Late, H. Morgan and C. S. Rout, *Nanoscale*, 7 (2015) 13293-13312.
11. B. G. Mahmoud, M. Khairy, F. A. Rashwan, C. W. Foster and C. E. Banks, *RSC Adv.*, 6 (2016) 14474–14482.
12. M. Khairy, N. A. Choudry, M. Oustai, D.K. Kampouris, R.O. Kadara and C. E. Banks, *ChemPhysChem.*, 11 (2010) 875–879 .
13. B. G. Mahmoud, M. Khairy, F. A. Rashwan, and C. E. Banks, *Anal. Chem.*, 89 (2017) 2170–2178
14. C. F. Thorna, T. E. Kleina and R.B. Altman, *Pharmacogenet Genom.*, 19 (2009) 556–558.
15. R.S Irwin, F.J. Curley and F. M. Bennett, *Drugs*. 46 (1993) 80-91.
16. V. Srinivasan, D. Wielbo, J. Simpkins, J. Karlix, K. Sloan and I. Tebbett, *Pharm Res.*, 13 (1996) 296-300.
17. S.C. Armstrong and K.L. Cozza, *Psychosomatics*, 44 (2003) 515–520.
18. Y. Fan, J.-H. Liu, H.-T. Lu and Q. Zhang, *Colloids Surf. B*, 85 (2011) 289–292.

- 19.A. C. Torres, M. M. Barsan and C.M.A. Brett, *Food Chem.*, 149 (2014) 215–220.
- 20.S. Suzen, C. Akay, and S.Cevheroglu, *Farmaco*, 54 (1999) 705–709.
- 21.E. Haffen, G. Paintaud, M. Berard, C. Masuyer, Y. Bechtel, and P. R. Bechtel, *Therapeutic Drug Monitoring*, 22 (2000) 258–265.
- 22.K. Masumoto, Y. Tashiro, K. Matsumoto, A. Yoshida, M. Hirayama, and S. Hayashi, *J. Chromatogr. B*, 381 (1986) 323–329.
- 23.M. R. Gomez, L. Sombra, R. A. Olsina, L. D. Mart´inez, and M. F. Silva, *Farmaco*, 60 (2005) 85–90.
- 24.B. Rezaei, T. Khayamian, and A. Mokhtari, *J. Pharm. Biomed. Anal.*, 49 (2009) 234–239.
- 25.N. R. Martos, A. M. Díaz, A. Navalón, I. D. O. Payà and L. F. C. Vallvey, *J. Pharm. Biomed. Anal.*, 23 (2000) 837–844.
- 26.L. Asturias-Arribas, M. A. Alonso-Lomillo, O. Domínguez-Renedo, M. J. Arcos-Martínez, *Talanta* 129 (2014) 315–319.
- 27.L. Asturias-Arribas, M. A. Alonso-Lomillo, O. Domínguez-Renedo, M. J. Arcos-Martínez, *Talanta*, 111 (2013) 8–12.
- 28.S. Jesny, K. Girish Kumar, *Electroanalysis*, 29 (2017) 1828 – 1837.
- 29.L. R. Cumba, J. P. Smith, K. Y. Zuway, O.B. Sutcliffe, D. R. do Carmo and C. E. Banks, *Anal. Methods*, 8 (2016) 142-152.
- 30.J. P. Smith, J. P. Metters, C. Irving, O. B. Sutcliffe, C. E. Banks, *Analyst*, 139 (2014) 389–400.
- 31.J. P. Metters, R. O. Kadara, C. E. Banks, *Analyst*, 136 (2011) 1067–1076.
- 32.N .Hernández-Ibáñez, L. García-Cruz, V. Montiel, C. W. Foster, C. E. Banks , *Biosens. Bioelectron.*, 77 (2016) 1168-1174.
- 33.M. Khairy, R. O. Kadara, D. K. Kampouris, C. E. Banks, *Anal. Methods*, 2 (2010) 645-649.
- 34.A. Hayat, D. Andreescu, G. Bulbul, S. Andreescu, *J. Colloid Interface Sci.*, 418 (2014) 240–245.
35. F. Rollin-Genetet, C. Seidel, E. Artells, M. Auffan, A. Thiéry, and C. Vidaud, *Chem Res Toxicol.* 28 (2015) 2304 – 2312.

36. A. B. Stambouli and E. Traversa, *Sust. Energ.*, 6 (2002) 433–455.
37. S. Patil, S. C. Kuiry, S. Seal and R. Vanfleet, *J. Nanopart.*, 4 (2002) 433–438.
38. G.A. Deluga, J.R. Salge, L.D. Schmidt and X. E. Verykios, *Science*, 303 (2004) 993–997.
39. K. Otsuka, T. Ushiyama and I. Yamanaka, *Chem. Lett.*, 9 (1993) 1517–1520.
40. A. Trovarelli, *Catal. Rev. Sci. Eng.*, 38 (1996) 439–520.
41. J. Kaspar, P. Fornasiero and M. Graziani, *Catal. Today*, 50 (1999) 285–298.
42. A. Corma, P. Atienzar, H. Garcia and J. Y. Chane-Ching, *Nat. Mater.*, 3 (2004) 394–397.
43. L. Celardo, J. Z. Pedersen, E. Traversa, and L. Ghibelli, *Nanoscale*, 3 (2011) 1411–1420.
44. H. Pang and C. Chen, *RSC Adv.*, 4 (2014) 14872–14878.
45. C. Xu and X. Qu, *NPG Asia Mater.*, 6 (2014) 90.
46. A. A. Ensafi, R. Noroozi, N. Zandi—Atashbar and B. Rezaei, *Sens. Actuators B*, 245 (2017) 980–987.
47. N. Padmanathan and S. Selladurai, *RSC Adv.*, 2014, 4, 6527–6534; M. Srivastava, A. K. Das, P. Khanra, M. E. Uddin, N. H. Kima and J. H. Lee, *J. Mater. Chem. A*, 1 (2013) 9792–9801.
48. M. Khairy, A. A. Khorshed, F. A. Rashwan, G. A. Salah, H. M. Abdel-Wadood and C. E. Banks, *Sens. Actuators B*, 252 (2017) 1045–1054.
49. S. Gogoi, H. Borah, R. R. Dutta and P. Puzari, *Phys. Chem. B*, 119 (2015) 4749 – 4757.
50. M. Khairy, A. A. Khorshed, F. A. Rashwan, G. A. Salah, H. M. Abdel-Wadood and C. E. Banks, *Sens. Actuators B*, 239 (2017) 768–775.
51. G. Jia, H. You, M. Yang, L. Zhang, and H. Zhang, *J. Phys. Chem. C* 113 (2009) 16638–16644.
52. Galus, Z.; *Fundamentals of Electrochemical Analysis*, 2<sup>nd</sup> ed., Ellis Horwood: New York, 1976.
53. L. Jiang, S. Gu, Y. Ding, F. Jiang and Z. Zhang, *Nanoscale*, 6 (2014) 207–214.
54. B. J. Sanghavi and A. K. Srivastava, *Electrochim. Acta.*, 55 (2010) 8638–8648.
55. M. H. Pournaghi-Azar and A. Saadatirad, *Electroanalysis*, 22 (2010) 1592 – 1598.
56. A. A. Ensafi, N. Ahmadi, B. Rezaei, and M. M. Abarghoui, *Talanta*, 134 (2014) 745–753.

57. B. Habibi, M. Abazari and M. H. Pournaghi-Azar, *Colloids Surf. B.*, 114 (2014) 89–95.
58. Y. Li, K. Li, G. Song, J. Liu, K. Zhang and B. Ye, *Sens. Actuators B.*, 182 (2013) 401–407.
59. L. Svorc, J. Sochr, J. Svitkova, M. Rievaj and D. Bustin, *Electrochim. Acta.*, 87 (2013) 503–510.
60. A. Afkhami, H. Khoshsafar, H. Bagheri and T. Madrakian, *Sens. Actuators B.*, 203 (2014) 909–918.
61. X. Chen, J. Zhu, Q. Xi and W. Yang, *Sens. Actuators B.*, 161 (2012) 648–654.
62. K. Tyszczuk-Rotko, I. Beczkowska, *Food Chem.*, 172 (2015) 24–29.
63. S. Yang, R. Yang, G. Li, L. Qu, J. Li and L. Yu, *J. Electroanal. Chem.*, 639 (2010) 77–82.
64. B. C. Lourencao, R. A. Medeiros, R. C. Rocha-Filho, L. H. Mazo, O. Fatibello-Filho, *Talanta*, 78 (2009) 748–752.
65. T. R. Saciloto, P. Cervini, É. T. G. Cavaleiro, *J. Braz. Chem. Soc.* 24 (2013) 1461–1468.

### Author Biographies

**Mohamed Khairy** received his PhD in Chemistry (Nanodevice) from Waseda University, Tokyo, Japan in 2013. He was a postdoc researcher at national institute for material science in 2014. Currently, he is working as lecturer in Chemistry Department, Faculty of Science, Sohag University, Sohag, Egypt. His current research interests are control synthesis of porous metal oxide nanostructures for energy and environmental applications.

**Bahaa G. Mahmoud** is chemist at clinical toxicology lab, Sohag University hospital. He is MSc student in Chemistry Department, Faculty of Science, Sohag University, Sohag, Egypt. His current research interests are control synthesis of metal oxide nanostructures for electrochemical sensor.

**Craig E. Banks** is a professor of Chemistry at Manchester Metropolitan University and has published over 342 papers with a h-index over 51 (Web of Science, July 2016). He has written 5 books, contributed 16 book chapters and is an inventor of 15 patents. Craig has elected as a highly cited researcher by Thomson Reuters; Listed in the World's Most Influential Scientific Minds 2014. Craig has also spun out two companies from his research. Craig was awarded the Harrison–Meldola Memorial Prize in 2011 for his contributions to the understanding of carbon materials, in particular graphene and its application as an electrode material. His current research is directed toward the pursuit of studying the fundamental understanding and applications of nano-electrochemical systems such as graphene, carbon nanotube and nanoparticle derived sensors and developing novel electrochemical sensors *via* screen printing and related techniques.

**Table 1:** Electrochemical impedance parameters for CeO<sub>2</sub>-SPE and SPE in in presence of 0.5 mM [Fe(CN)<sub>6</sub>]<sup>3-/4-</sup>/ 0.1 M KCl deduced from equivalent circuit.

Parameters	SPE	CeO <sub>2</sub> -SPE
<b>R1 (<math>\Omega</math>)</b>	869	954
<b>R2 (<math>\Omega</math>)</b>	80000	38129
<b>W (<math>\Omega s^{-1/2}</math>)</b>	85818	30851
<b>P1(F)</b>	$1.1 \times 10^{-5}$	$1.7 \times 10^{-6}$
<b>n1</b>	0.92	0.82

**Table 2:** The proposed CeO<sub>2</sub>-SPE as nonenzyme sensor in comparison with previous reported

Electrode	Target Molecule	Linear Range (μM)	LOD (μM)	Supporting electrolyte	Applicability	Reference	comment
EGR/ZnO/GCE	APAP	0.02 – 10	33	0.1 M Phosphate buffer pH 6.0	Tablet and human serum	53	-Tedious fabrication process -Difficult to apply in-field with high LOD -Expensive electrode materials -Polishing is needed
ISSMCNT-PE	APAP CAF	0.291-62.7 0.291-62.7	0.258 0.0883	phosphate buffer solution pH 7	Tablet, coffee beverages, urine and blood serum	54	-Electrode Poisoning with time -Difficult to apply in-field -Electrode fouling and Poisoning with time -lower linear concentration range.
Thin layer palladium/Al	APAP COD	100-3000 100-3000	5 5	0.25 M KNO <sub>3</sub> + 0.5 M acetate of pH 6	Tablet	55	-Tedious fabrication process -Difficult to apply in-field -Expensive electrode materials -Polishing is needed
Psi/Pd-NS/CNTPE	APAP COD	1-700 1-700	0.4 0.3	Britton-Robinson buffer at pH 7	Tablet, urine and plasma samples	56	-Electrode Poisoning with time -Multi-step fabrication processes -Difficult to apply in-field -Expensive electrode materials -Polishing is needed
SWCNT/CCE	COD CAF	0.2-230 0.4-300	0.11 0.25	0.01 M H <sub>2</sub> SO <sub>4</sub> pH 1.7	Tablets and urine	57	-Electrode Poisoning with time -Tedious fabrication process -Difficult to apply in-field -Small linear concentration range -Expensive electrode materials -Polishing is needed
GR/Nafion/GCE	COD	0.05-30	0.015	Phosphate buffer pH 4	Urine	58	-Electrode Poisoning with time -Tedious fabrication process -Difficult to apply in-field -Small linear concentration range -Polishing is needed
BDD/Film electrode	COD	0.1-0.6	0.08	Britton-Robinson buffer at pH 7	Tablets and urine	59	-Electrode Poisoning with time -Tedious pre-treatment processes -Small linear concentration range -Polishing is needed
GR/CoFe <sub>2</sub> O <sub>4</sub> /CPE	APAP COD	0.03-12 0.03-12	0.025 0.011	Britton Robinson buffer pH 7	Tablet, urine and plasma	60	-Electrode Poisoning with time -Multi-step fabrication processes -Difficult to apply in-field -Small linear concentration range -pre-treatment and Polishing is needed -electrode poisoning and fouling with time
SWCNT/GNS/GCE	APAP	0.05-64.5	0.038	Phosphate buffer pH 7	Human serum	61	-Multi-step fabrication processes -Difficult to apply in-field -Expensive electrode materials -Polishing is needed
Nafion covered lead film electrode	CAF	0.995-10.6	0.798	0.1 mol L <sup>-1</sup> H <sub>2</sub> SO <sub>4</sub>	Tea, coffee, soft and energy drink samples	62	-Electrode Poisoning with time -Tedious fabrication process -Difficult to apply in-field -Toxic electrode materials -Polishing is needed
Nafion/MWNTs/CPE	CAF	0.6-400	0.23	0.01 mol L <sup>-1</sup> H <sub>2</sub> SO <sub>4</sub> pH 2	Beverage samples	63	-Electrode Poisoning with time -Difficult to apply in-field -Expensive electrode materials -Polishing is needed
BDD	APAP CAF	0.5-83 0.5-83	0.49 0.053	Acetate buffer, pH 4.5	Tablets	64	-Electrode Poisoning with time -No swelling during analysis in aqueous media -Small linear concentration range -Electrode Poisoning with time
Polyurethane-SPEs	APAP CAF	1.00 - 40.0 4.00 - 200	0.84 1.6	phosphate buffer pH 6.0	Tablets	65	-Large-scale electrode production -Simple fabrication process -Wide linear concentration range -Reproducible and stable electrode in real samples - No need any pretreatment - disposable electrode -Economic electrode materials -Could measure APAP, COD and CAF simultaneously for on-site field analysis
CeO <sub>2</sub> -SPEs	APAP COD CAF	0.09 – 7.0 0.09 – 50.0 5 – 286	0.051 0.043 2.4	Britton Robinson buffer pH 2	Human serum	This work	

BDD boron doped diamond, MWNT multi walled carbon nanotube, SWCNT/GNS Single-walled carbon nanotube –graphene nanosheet hybrid film modified glassy carbon electrode, SWCNT/CCE Single-walled carbon nanotubes modified carbon-ceramic electrode, GR reduced graphene, Psi/Pd NS/ CNTPE porous silicon/palladium nanostructure Carbon nanotube paste electrode, ISSM-CNT-PE surfactant-modified multiwalled carbon nanotube paste electrode.

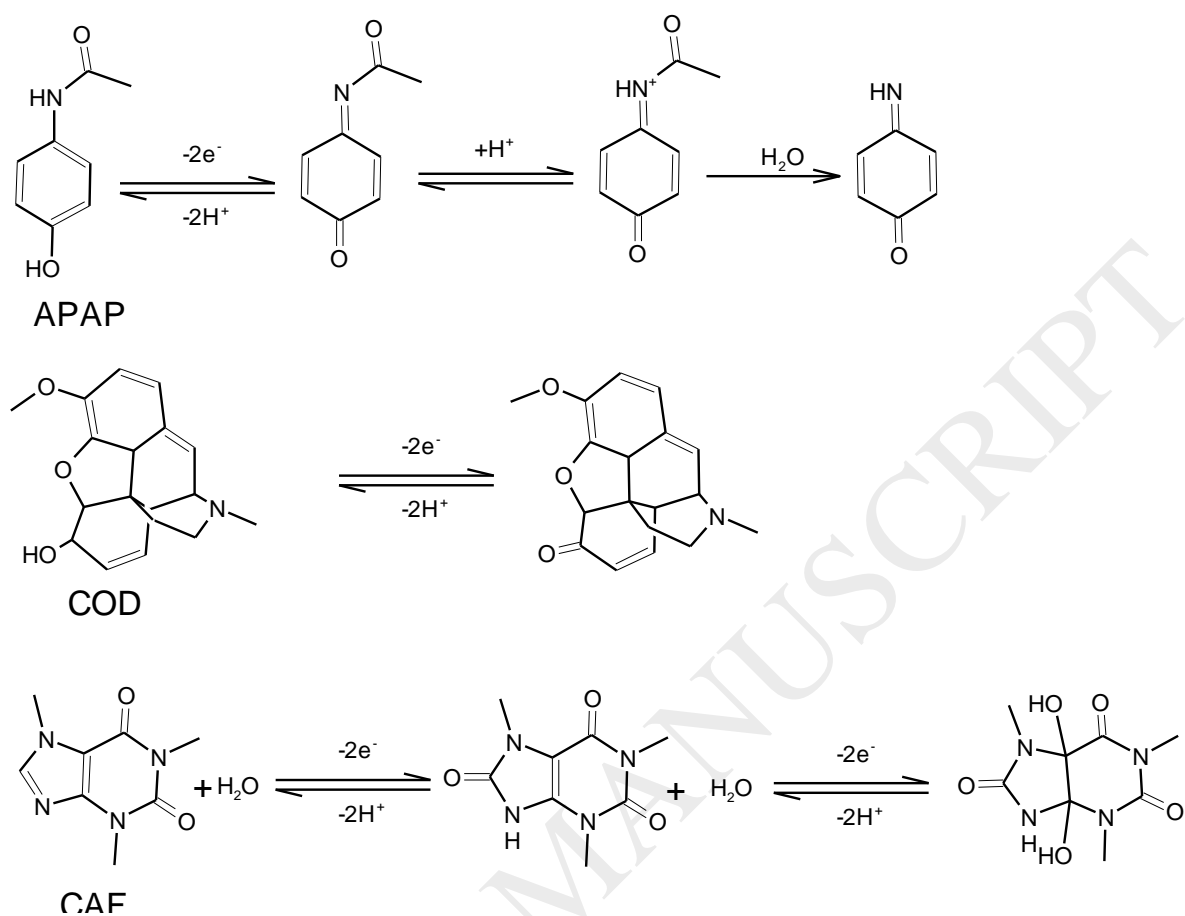
**Table 3.** Sensitive determinations of APAP, COD and CAF in human serum samples.

Blood	Added ( $\mu\text{M}$ )			Detected ( $\mu\text{M}$ )			Recovery (%) $\pm$ SD <sup>a</sup>		
	APAP	COD	CAF	APAP	COD	CAF	APAP	COD	CAF
serum									
Sample 1	60.0	60.0	40.0	59.17	59.45	40.80	98 $\pm$ 1.23	99 $\pm$ 4.07	102 $\pm$ 2.91
	75.0	75.0	80.0	73.30	75.90	80.60	97.7 $\pm$ 3.7	101 $\pm$ 2.5	100.7 $\pm$ 1.08
Sample 2	185.0	185.0	120.0	189.80	190.0	118.9	102 $\pm$ 4.40	102 $\pm$ 3.4	99.06 $\pm$ 3.03
	200.0	190.0	160.0	202.49	190.80	161.4	101 $\pm$ 2.01	100.4 $\pm$ 3.5	100.8 $\pm$ 2.87

<sup>a</sup> Relative standard deviation of three determinations

**List of Tables**

## List of Figures and schemes

**Scheme 1.** Electrochemical oxidation mechanisms of APAP, COD and CAF molecules.

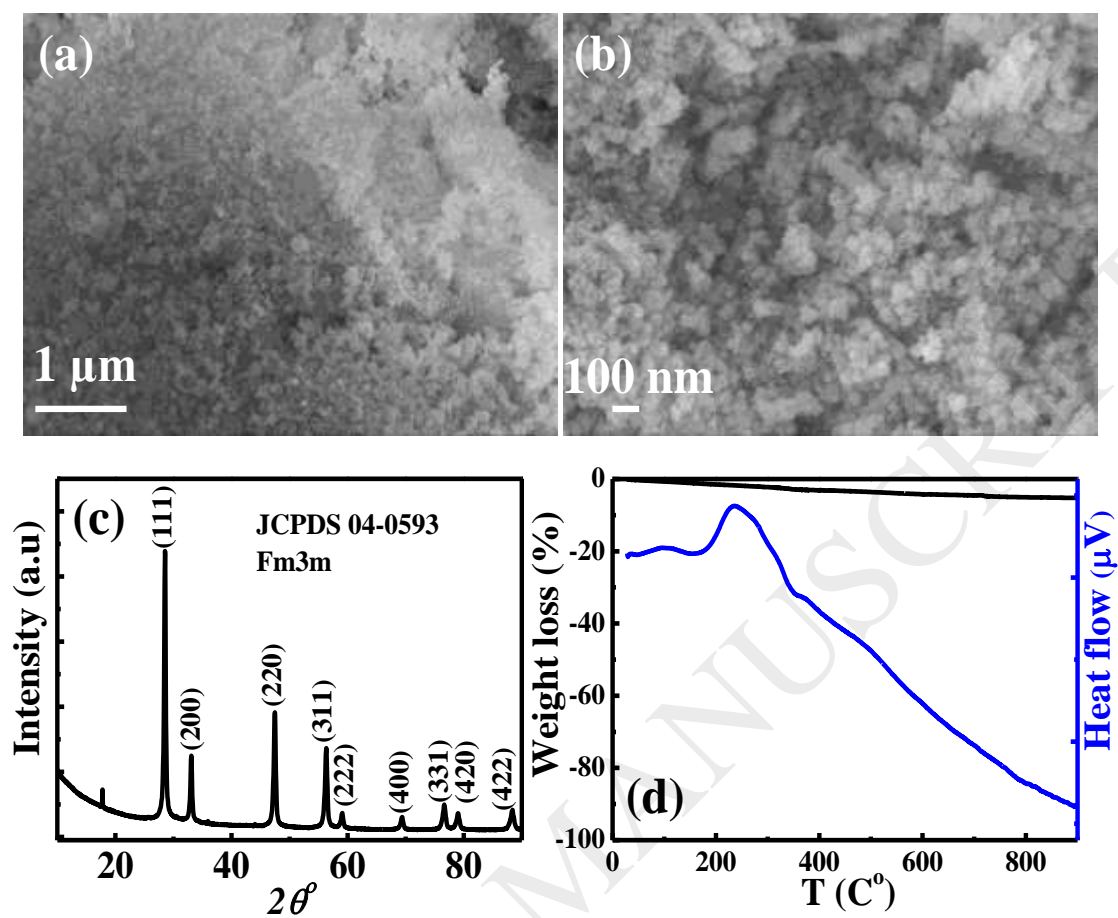


**Figure 1.** (a and b) FE-SEM images, (c) X-ray powder diffraction pattern and (d) TGA of cerium oxide nanostructures prepared via a simple hydrothermal treatment within acidic medium.

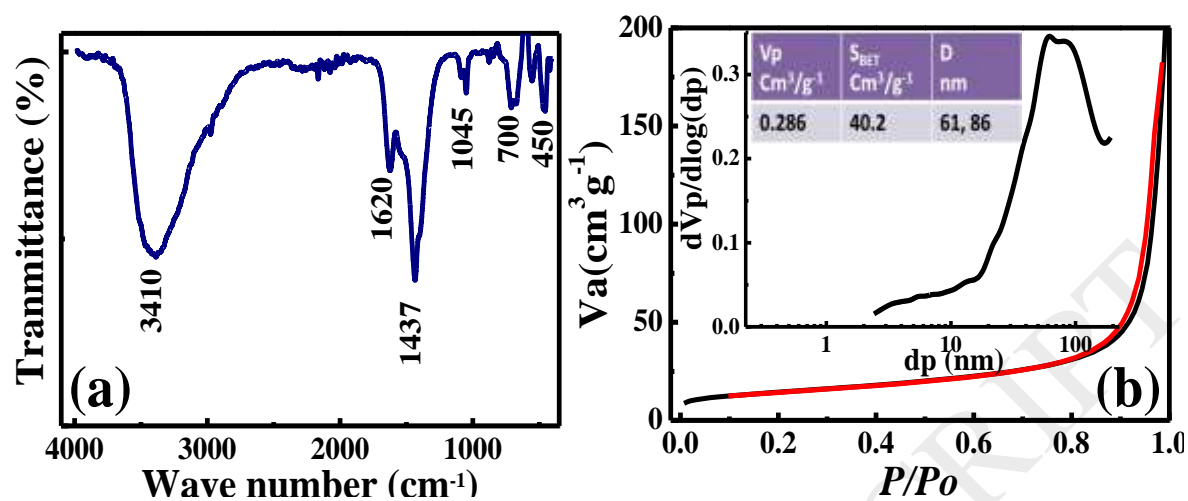


**Figure 2.** (a) FTIR and (b)  $\text{N}_2$  adsorption/desorption isotherms of  $\text{CeO}_2$  nanostructures [Inset: corresponding BJH pore distribution curve].

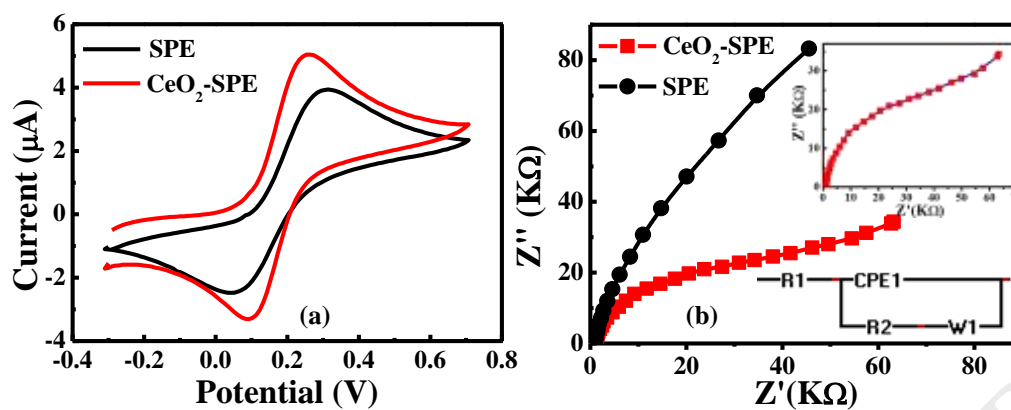


**Figure 3.** (a) Cyclic voltammetric curves at scan rate 50 mVs<sup>-1</sup> and (b) Nyquist plot including equivalent circuit of SPE and CeO<sub>2</sub>-SPE in presence of 0.5 mM [Fe(CN)<sub>6</sub>]<sup>3-/4-</sup> in 0.1 M KCl. Inset Fig. 3b Randles's equivalent circuit].

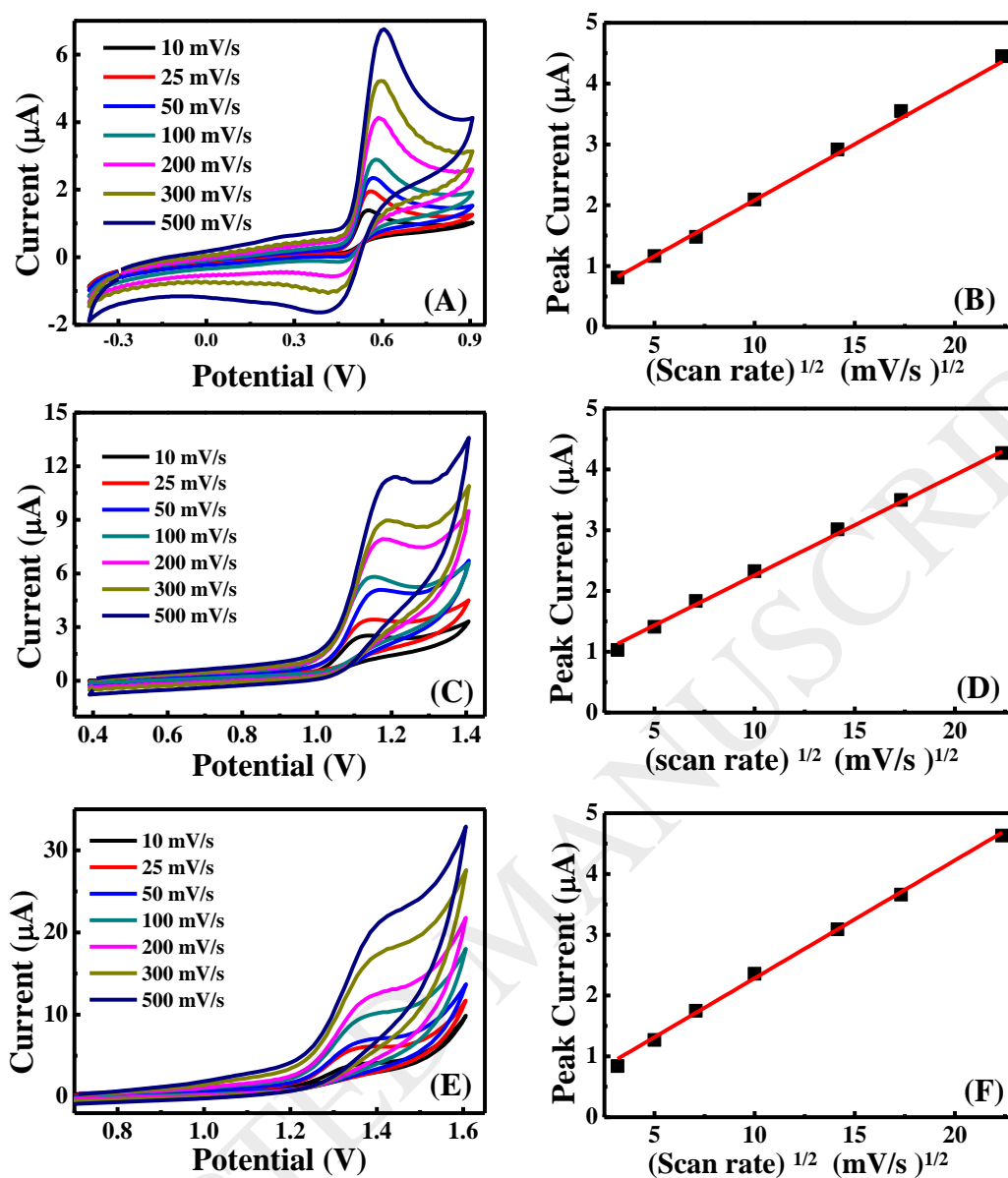


**Figure 4.** (A) Effect of voltammetric scan rates upon the cyclic voltammetric responses of 100  $\mu\text{M}$  of APAP, (C) 200  $\mu\text{M}$  of COD and (E) 200  $\mu\text{M}$  CAF observed on  $\text{CeO}_2$ -SPE in B.R. buffer pH 2, (B, D and F) Dependence of peak current of APAP, COD and CAF on the square root of scan rates.

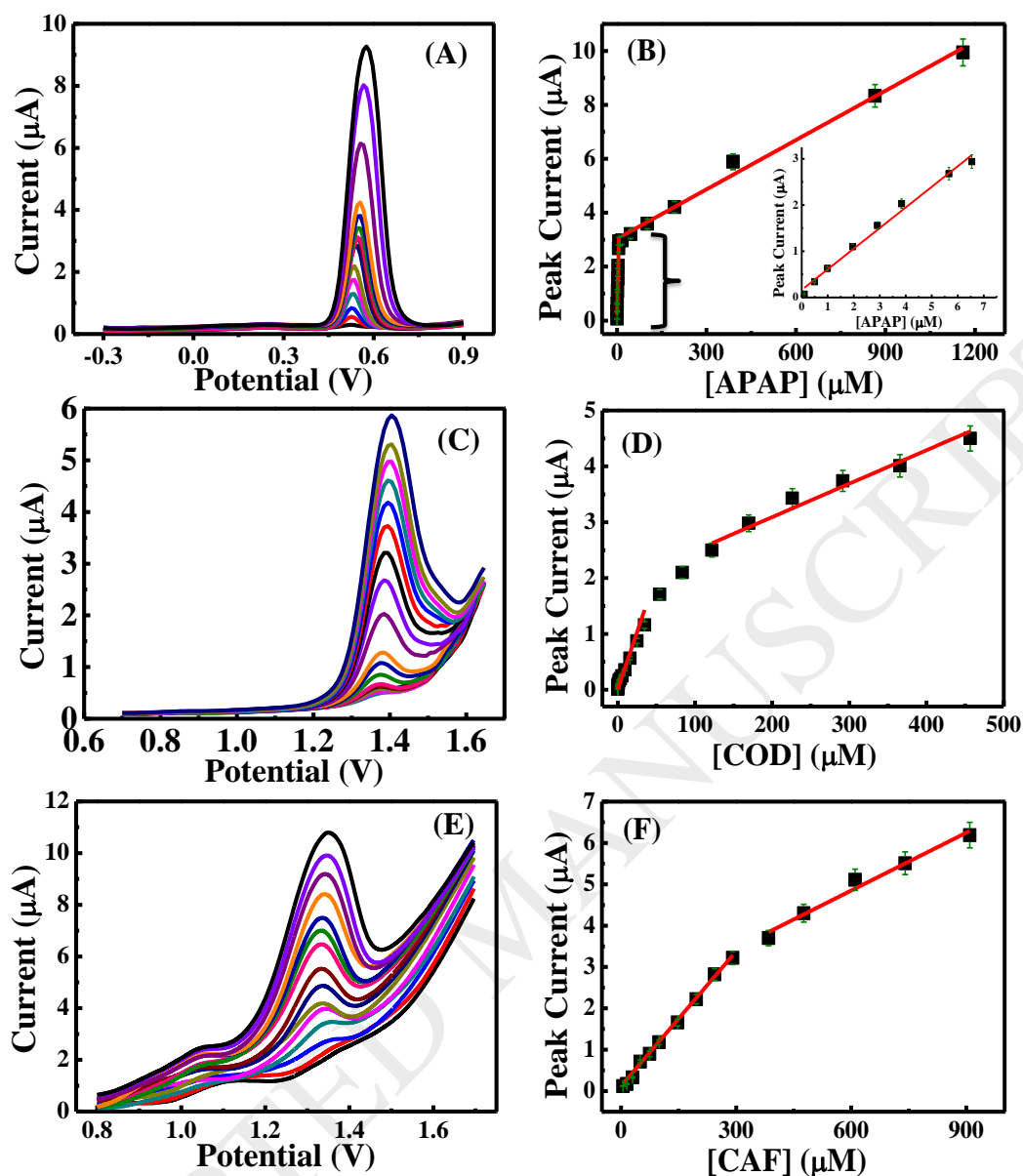


**Figure 5.** (A) Differential pulse voltammetric responses of successive additions of APAP, (C) COD and (E) CAF into B.R. buffer pH 2 on CeO<sub>2</sub>-SPE, (B, D, F) Typical calibration plots corresponding to APAP, COD and CAF additions. [DPV parameters : step potential 0.01 V, modulation potential 0.025 V, modulation time 0.05 s, interval time 0.2 s, scan rate 50 mVs<sup>-1</sup>, deposition time 20 s and equilibrium time 20 s].

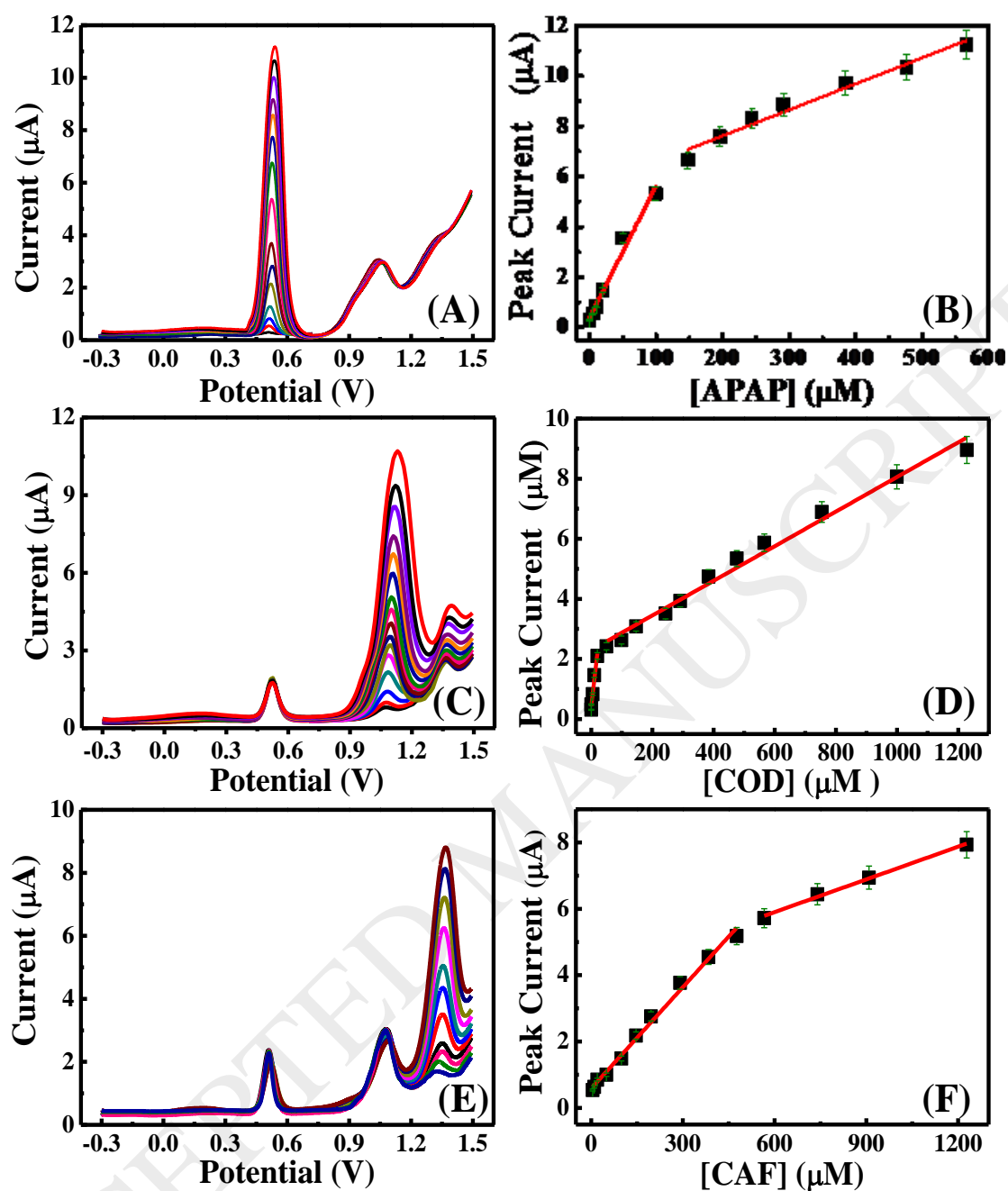


**Figure 6.** (A) Differential pulse voltammetric curves for successive addition of APAP in presence 50  $\mu\text{M}$  COD and 50  $\mu\text{M}$  CAF, (B) Corresponding peak current as function of APAP concentrations. (C) Differential pulse voltammetric curves for successive addition of COD in presence 50  $\mu\text{M}$  APAP and 50  $\mu\text{M}$  CAF, (D) Corresponding peak current as function of COD concentrations, (E) Differential pulse voltammetric curves for successive addition of CAF in presence 50  $\mu\text{M}$  APAP and 50  $\mu\text{M}$  COD and (F) Corresponding peak current as function of CAF concentration. [DPV parameters: step potential 0.01 V, modulation potential 0.025 V, modulation time 0.05 s, interval time 0.2 s, scan rate 50  $\text{mVs}^{-1}$ , deposition time 20 s and equilibrium time 20 s].

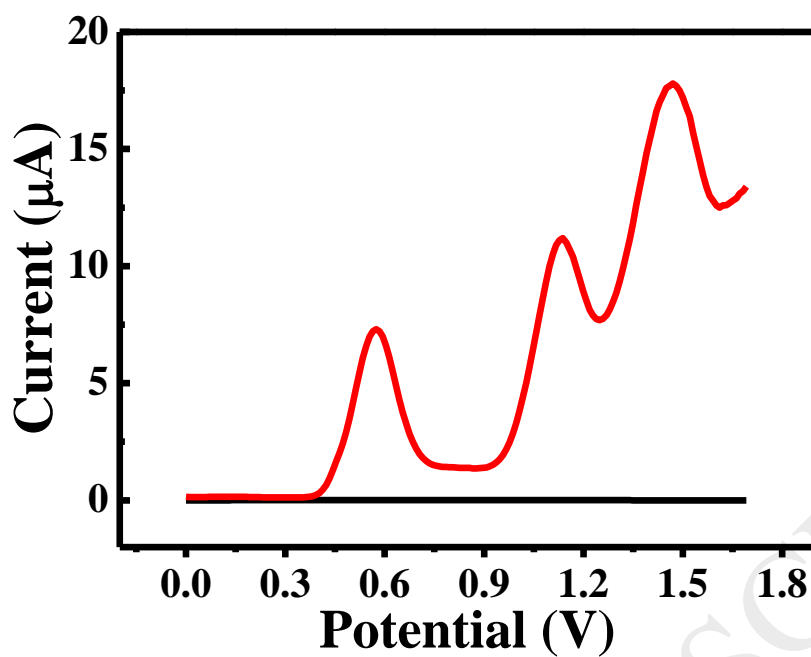


**Figure 7.** Differential pulse voltammetric response of 200  $\mu\text{M}$  of each APAP, 1.0 mM COD and 1.0 mM CAF in human serum samples measured onto 3-electrodes configuration of graphite SPE. [DPV parameters: step potential 0.01 V, modulation potential 0.025 V, modulation time 0.05 s, interval time 0.2 s, scan rate  $50 \text{ mVs}^{-1}$ , deposition time 20 s and equilibrium time 20 s].